Journal of Alloys and Compounds, 195 (1993) 695–702
JALCOM 7561

$YBa_2Cu_3O_7$ Devices Grown by Evaporation

R.G.Humphreys, J.S.Satchell, N.G.Chew, J.A.Edwards, S.W.Goodyear and M.N.Keene

DRA, Malvern, Worcestershire WR14 3PS, UK

Abstract

Fabrication techniques for all-epitaxial $YBa_2Cu_3O_7$ thin film devices and results obtained on Josephson junctions, SQUIDs and junction arrays are described.

1. Introduction

High temperature superconductor thin film devices differ from all other solid state devices in that material growth and device fabrication cannot be treated separately. Growth and patterning steps must be interleaved, so it is important to make devices at the earliest possible stage in the development of the technology so that the processes turn out compatible. For a realistic circuit technology, we need to develop the ability to make not only patterned single layer films, but also ground planed circuits and low leakage insulated cross-overs as well as reproducible and controllable Josephson junctions. Devices based on the growth of a ground plane on the back of the substrate[1] are gradually becoming more widespread, but the microwave designers are still pressing for thinner substrates and larger areas. Although impressive results have been obtained with more complex circuits[2], reproducibility and yield still leave much to be desired. In this paper, we describe our recent work on device technology.

2. Technology

Despite early worrries about the effects of water on high temperature superconductors, it has turned out that standard photolithography with positive resist and aqueous solutions works without adaptation. Wet etching has been widely used for simple patterning, but the need for better reproducibility, lack of residues, and ability to stop processing at arbitrary depth has led to dry etching being preferred for more complex structures[2]. Since no suitable reactive dry etching scheme has been found, ion milling is the only alternative. As the structures being fabricated become more complex, it becomes more critical to monitor the milling so that it can be stopped at the optimum time, i.e. detecting the end point. The most widely used approach is simply to calibrate the milling rates, and to mill under carefully controlled conditions for a defined period of time. However, the milling rate is not always accurately predictable, and considerable tolerance margins have to be built into device structures to allow for variations.

We use an *in-situ* secondary ion mass spectrometry (SIMS) system, described in more detail elsewhere[3], to give depth information during the patterning process. A mass spectrometer located in the milling chamber detects the secondary ions produced during milling. The species monitored routinely are $^{89}Y^+$, $^{138}Ba^+$, $^{63}Cu^+$, $^{141}Pr^+$ and $^{24}Mg^+$.

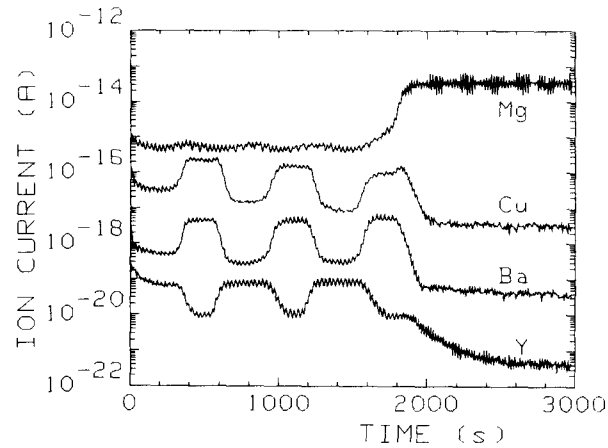

Fig. 1 SIMS trace on milling through a $YBa_2Cu_3O_7$-Y_2O_3 multilayer. The layer thicknesses were 20nm. For clarity, the Ba and Y curves have been shifted downwards by 2 and 4 decades respectively.

The results obtained are illustrated using an epitaxial multilayer stack comprising six alternating 20nm thick layers of $YBa_2Cu_3O_7$ and Y_2O_3 on an MgO substrate. This structure was milled using 500eV A^+ ions at an ion current density of $\sim 0.2 mA/cm^2$ and an angle of incidence 10° from the substrate normal. The sample was rotated at ~ 0.1 Hz during milling. The resulting data are shown in fig. 1. The presence of the separate layers is abundantly

0925-8388/93/$06.00

clear, with about an order of magnitude of contrast in the signals between materials. The milling rates of Y_2O_3 and $YBa_2Cu_3O_7$ are estimated to be close to a ratio 2:3 from these results. The depth resolution given by the width of the interfaces between layers is ~4nm. The rapid oscillations in the signal are associated with the sample rotation, which has been deliberately chosen to be asynchronous with the sampling period of the mass spectrometer to avoid slow beating effects which could confuse the identification of an end point.

After ion milling, our material requires annealing in oxygen to restore the critical current density to approximately the value before patterning.This is not true of all types of material. We have milled narrow tracks from a laser ablated film grown by NKT[4]. This showed a high critical current density (~4 10^6 A/cm^2) after milling, which fell on annealing, in direct contrast to the behaviour of our evaporated films, despite identical processing. We conclude that different growth techniques can yield different sorts of material, and a process which is optimised for one type of material will not necessarily work without modification on another.

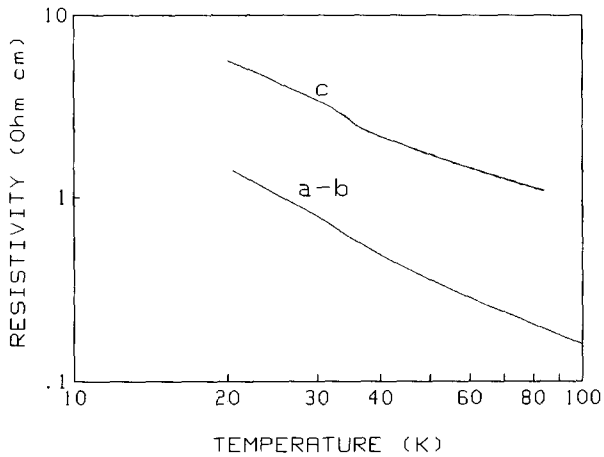

Fig. 2 Resistivity of $PrBa_2Cu_3O_7$ films measured parallel to the c-axis between superconducting electrodes (c), and in the film plane (a-b). The two films were made in the same growth run.

Many groups have reported successful mutual epitaxy between superconducting and insulating layers, but making the insulators pinhole free is less easy. The most widespread success has been achieved with $SrTiO_3$ as the insulator[2]. We have previously described some of the problems ecountered in achieving good isolation using Y_2O_3[5]. For use in flux transformers, high insulation resistance is not required, and we are exploring the use of $PrBa_2Cu_3O_7$ as the insulator material for this application. This has the advantage of having the same crystal structure and phase transition as the superconductor, as well as being permeable to oxygen. Fig.2 shows the resistivity of this material measured in a cross-over structure between layers of $YBa_2Cu_3O_7$, and in a conventional 4-terminal experiment. With a c-axis resistivity of this magnitude, we expect an isolation resistance of ~20mΩ for a typical washer SQUID structure at high temperatures. This is expected to damp the undesirable microwave resonances of the structure, but will add significant Johnson noise to the flux transformer signal, at least for a 3-layer magnetometer design[6]. A higher resisitivity would be preferred. Our data are only preliminary, but we are led to believe improvements may be possible by the much (~20 times) higher in-plane resistivities measured by Obara et al.[7]

The other key step in making circuits is the ability to make superconducting connections between layers. Fig. 3 shows a schematic of a test structure to demonstrate the technology required for a flux transformer including window connections through an insulator and current flow over multiple steps.

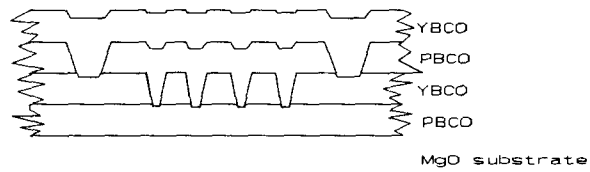

Fig. 3 Schematic of the test structure used for superconducting interconnects.

The structure was grown on a buffer layer of $PrBa_2Cu_3O_7$ (PBCO) to inhibit growth of 45° rotated $YBa_2Cu_3O_7$ (YBCO). The first YBCO layer was grown on top of the PBCO in the same growth run. An array of fifteen 30μm wide stripes separated by 30μm was patterned across a small section of the YBCO to simulate the coil of a flux transformer. Next a 0.4μm layer of PBCO was grown as an insulator over the structure. Two windows 100x250 μm were opened up in the PBCO either side of the stripes and milled down into the lower YBCO layer. The final growth step was to deposit an upper YBCO layer, 0.35μm thick, which made contact with the lower YBCO layer through the windows in the PBCO. This top layer was patterned into a 250μm wide track between the two windows which crossed the strips perpendicular to the 15 undulations. The sample was then patterned with a circular arc 250 μm wide and 8 mm diameter which started and ended at the windows. It was then milled down through the three PBCO/YBCO/PBCO layers to give the fully patterned ring with two superconducting interconnects and 15 undulations.

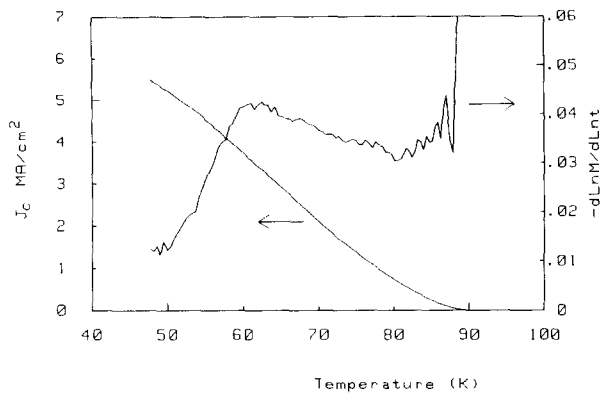

Fig. 4 Critical current density and normalised rate of decay of magnetisation for the test structure as functions of temperature.

A persistent current was set up in the ring by applying a short magnetic field pulse, and its magnitude was measured by observing the associated magnetic field using an InSb Hall sensor[8]. The ring was found to support a macroscopic circulating current, having a transition temperature of 90K. At 77K the measured critical current density is 1.3×10^6 A/cm^2, which is within a factor of two of our standard single layer YBCO films. This measurement of J_c has a rather stringent voltage criterion of order 10^{-9} V, so this result is a good demonstration of the current carrying capacity of a join between two superconductors. Although the magnetisation decay process is not well understood, we note that the behaviour shown in Fig. 4 is different from that measured in unpatterned films.

Despite this progress, our magnetometers do not yet work. The problem is not with making superconducting interconnects. It is the presence of pinholes in the insulator which short out the flux transformer.

3. Junctions

Making Josephson junctions in high temperature superconductors has been the subject of intensive investigation worldwide[9-11]. So far an ideal solution has not been found, the key problems being reproducibility and controllability, particularly at the high critical current densities required for high temperature operation. We describe here results of experiments on step junctions on MgO substrates.

The junction technology we use has been described elsewhere[12]. Briefly, steps were made in an (001) MgO substrate either by wet etching or ion milling using a photoresist mask. A buffer layer of MgO 10nm thick was then grown by evaporation, followed by a 0.35μm film of $YBa_2Cu_3O_7$. The film was masked with photoresist and ion milled away except for narrow tracks crossing the step. The nature of the growth of $YBa_2Cu_3O_7$ on MgO is different from that on perovskite substrates[10] in that the c-axis grows approximately perpendicular to the local substrate surface. The devices were therefore made up of at least two tilt grain boundaries separated by the length of the step.

The electrical measurements were made in a continuous flow cryostat surrounded by double mumetal shields, which reduce the background field to about 1μT. The sample position is surrounded by a pair of coils in a quasi-Helmholtz configuration. The down leads pass through cold RLC low pass filters. A separate coaxial downlead terminates in a loop antenna and provides a method of introducing microwave radiation (8-12 GHz) into the system. The measurement electronics consists of a low noise differential preamplifier (with bootstrapped power supply) and low noise pseudo balanced current source mounted near the cryostat. These are connected to the control box, which contains the analogue sweep generator, current source for the magnetic field coils, buffered output stages, and a feedback loop to allow critical current at constant voltage to be determined as a function of magnetic field. The buffered, high level (+/- 10V) outputs are fed to a fast DVM through a multiplexer, and a computer can acquire the data in real time. A standard magnetic field sweep, for example, contained 500 points and was completed in 30s.

The temperature at which junctions first show a critical current is systematically lower than the T_c of the electrodes by an amount which correlates with junction strength. This is expected, and is due to thermal fluctuations. The junctions are overdamped at high temperatures, and have a temperature independent R_N. Many of the weaker junctions become hysteretic at low temperatures. Of the many junctions we have made, only a rather small fraction have shown well defined periods in their field dependence, and only these have been analysed in any detail. Fig. 5 shows a series of plots of the dependence of the critical current on magnetic field for one of the "best" of these. At low temperature, the oscillations are nearly triangular, characteristic of long junction behaviour[13].

As the temperature rises, the critical current drops and the oscillations become rounded and deeper. The field sweeps in the figure have been limited to ranges which do not cause flux jumps, and the width of this region decreases with increasing temperature. Near T_c wide field sweeps again become possible without abrupt flux jumps being evident, presumably due to flux entry becoming revers-

ible. In between these two regimes, we can identify a range of temperatures where the period is well defined. The junction of fig. 5 is so strongly coupled that only the curves at 85 and 88K appear to be free of long junction effects, and that at 81K is on the borderline. Successive minima show similar spacings, although in some cases even and odd peaks have different widths, and there is a weak trend towards greater peak width at large fields. The central peak width is expected to be more sensitive to large scale non-uniformity, and it is in fact found to be rather variable. A theory descibing the effect of magnetic fields in this junction geometry and the short junction limit has recently been developed, and shown to predict the measured period of the oscillations[14].

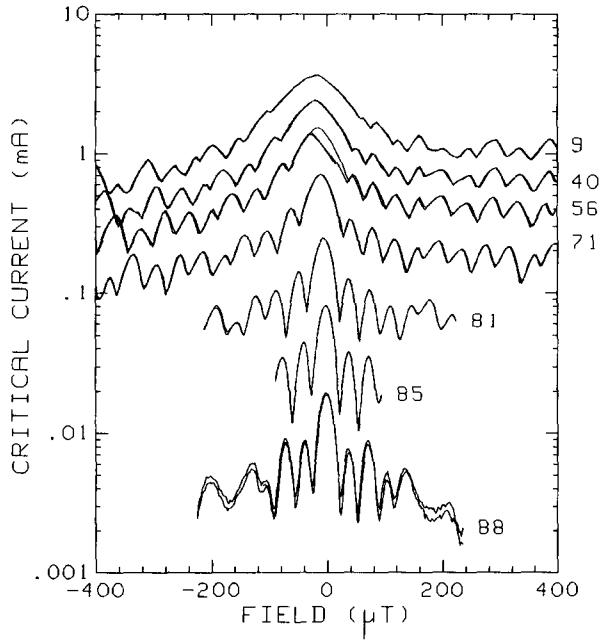

Fig.5 Critical current as a function of applied magnetic field for a 12μm wide junction measured at the temperatures indicated. Complete field sweeps are shown in all cases to indicate the amount of hysteresis.

The application of a magnetic field is a useful techniuqe for examining the uniformity of individual junctions, but the reproducibility of junction strength is best studied using series arrays. We show here the results of an array consisting of 100 junctions, each 5 μm wide. At low temperatures (<10K) most of the individual junctions were hysteretic, but the spread in critical currents is so large that at most only a few hysteresis loops interpenetrate. At 25K, the IV curve reveals many sharp breaks, although the hysteresis has now disappeared. The differential resistance as a function of current (fig.3) shows many well resolved critical currents. Some may correspond to more than one junction. The data stop when the preamplifier overloads, at a total array voltage of 120mV, although we presume that there are many more critical currents that we have not yet reached. There is no possibility of such an array synchronising itself in emission. If a microwave field is applied, Shapiro steps can be seen for the weakest junction by itself. At higher powers the external field may be able to synchronise the first two junctions, but there are no signs of giant steps.

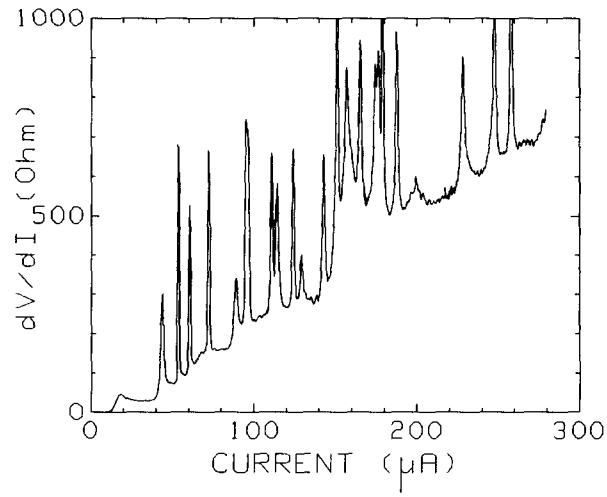

Fig. 6 Differential resistance as a function of current at 25K for a series array of 100 junctions each 5μm wide.

Although many of our individual junctions showed Shapiro steps at low microwave fields (see fig. 7) , some did not. This includes devices with well defined periods in a magnetic field. In these cases, Shapiro steps were weakly visible only when the critical current had been completely suppressed by the microwaves.

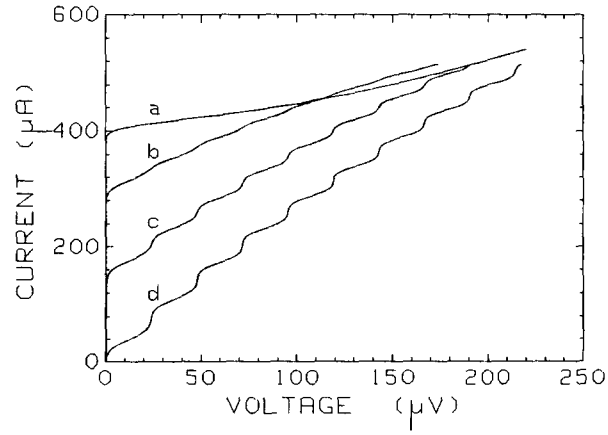

Fig. 7 Current-voltage characteristics of a 12μm wide junction measured at 75K with (b-d) and without (a) 11.5 GHz radiation. The microwave power increases from b to d.

4. SQUIDs

These junctions have been used as the active elements in SQUIDs. We describe here results on only two devices, but a more comprehensive set of results has been presented elsewhere[6]. They are small square structures with Josephson junctions on two opposing sides and superconducting tracks leading from the remaining two sides, designed to be a calculable geometry. The junctions are nominally 3μm wide but some are slightly thinner due to variations in the patterning method used. The chip layout is sparse, so that flux focusing by the remote electrodes is minimal ($\sim 1\%$).

The SQUIDs were measured in a specially adapted continuous flow cryostat which had slotted heat shields to reduce eddy currents. The cryostat was mounted in three concentric mu-metal shields, and all thermometry and heater wires were very heavily filtered. The devices were

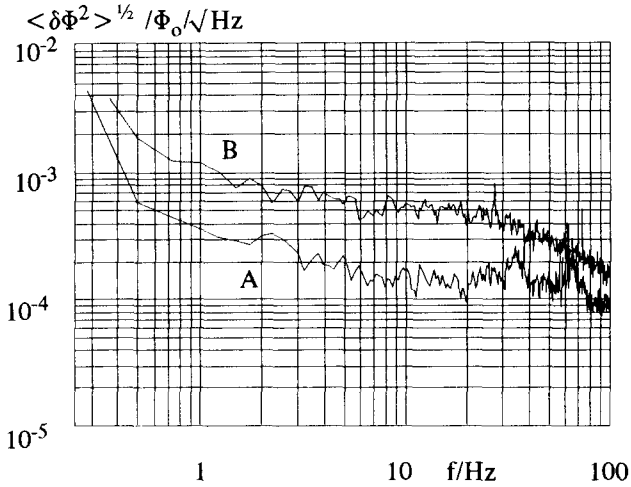

Fig 8. Magnetic flux noise performance of two SQUIDs. A, $(48\mu)^2$, 128 pH measured at 70.3 K. No significant increase of the noise was observed at 77K. B $(24\mu m)^2$, 66pH also measured at 70.3 K and exhibits a Lorentzian form consistent with the telegraph noise real time signal.

mounted on a Tufnol holder and surrounded by a mu-metal can which is optimised for 77K use. Within the can is a thermometer (which has no measurable effect on the SQUIDs), a Helmholtz coil set to apply known fields to the devices and an inductor-capacitor tank circuit for SQUID readout. All wires into the can pass through cooled filters.

The SQUID readout consisted of a very low-noise battery operated preamplifier. The signal was fed into a dual-phase lock-in amplifier whose outputs were connected to a spectrum analyzer. Current bias was provided by a mercury cell and resistor network, and flux modulation by an oscillator and resistor network. After each noise measurement the SQUID was biased below the critical current to determine the electronics noise. For many devices the use of the cooled tank circuit was unnecessary because the preamplifier was sufficiently low-noise (0.35nV/$\sqrt{}$Hz).

Fig. 8 shows the noise performance of two SQUIDS. We find that the noise is principally magnetic in origin for all our SQUIDs in the 0-70 Hz frequency range. This can be distinguished from voltage noise fluctuations by comparing the in-phase signal with the out of phase signal from the lock-in amplifier[15]. Critical current fluctuations, which are believed to be a major contributor to the 1/f spectrum, lead to current fluctuations around the SQUID ring and are therefore manifest as magnetic noise. Likewise, the motion of trapped flux lines in the body of the SQUID also contributes magnetic noise.

Although there is a significant spread in the critical currents of SQUIDs found on a single chip and a wide spread in the flux-to-voltage ratio, the distribution of critical currents is sufficiently narrow that all devices on a single chip demonstrate SQUID action at the same temperature. There is a wider spread in the critical currents between chips. For devices to be designed to work at a specified temperature, big improvements in junction reproducibility are required.

We observe no systematic correlation of magnetic flux noise with the temperature at which the SQUID is operating. At a given frequency the total spread of flux noise over all our devices under optimum conditions is about one order of magnitude. This behaviour is consistent with the noise being dominated by either flux motion[16] or traps in the junction. Both are likely to have a wide distribution of characteristic energies, and are capable of exhibiting random telegraph noise which we often observe.

5. Parallel junction arrays

Although the junction technology is still immature, it is not too early to explore what uses can be made of them in more complex configurations, as only in this way can we define the goals of the technology.

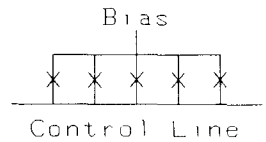

Fig 9. Schematic of the 4 loop VFT.

Parallel junction arrays form the basis of the vortex flow transistor (VFT). The devices are simply multi-loop SQUIDs, with provision for a control current to introduce flux into the loops. Our version (fig. 9) is a three terminal device[17] with the control current passing along one side of the loops, rather than the Wisconsin designs which have a separate control line[18]. Their design uses flux flow in thinned regions of superconductor, while we use step junctions. Large gain requires both deep modulation of the critical current by the control flux, and efficient coupling of the control current to the loops. Our earlier devices showed low current gain due to poor coupling of the control current to flux in the loops. We have revised the design by shortening the tracks containing the junctions to 6μm and using a narrower (higher inductance) control line. This has a significant side effect, which was not fully taken into account in our present design. The self flux from the junction currents becomes important at lower nominal values of β_l, and results in reduced values of peak critical current, less modulation of critical current and hence some loss of gain.

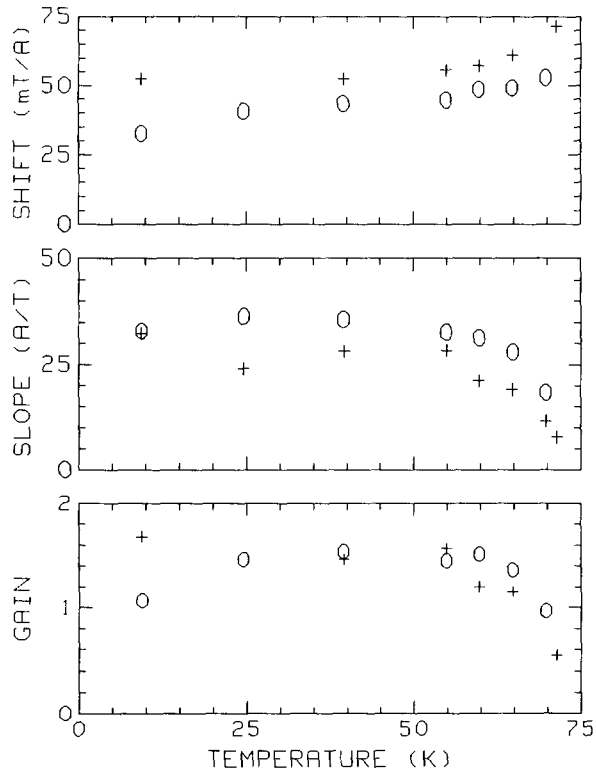

Fig. 10 Results for four loop (+) and five loop (O) VFTs as functions of temperature. Top panel shows the shift of the I_c B pattern with control current in mT/A. The middle graph gives the largest value of dI_c/dB from the same data. The current gain is shown at the bottom. Voltage gain is not shown as it depends on source and load impedances.

The devices studied most extensively had four or five loops and five or six junctions respectively. In both cases the total device length was 60μm. The junction width was 3μm. A connection was bought out from each end of the control line, and a control current could be injected giving transistor action. The bias current was extracted symmetrically through both connections. We measure the critical current as a function of applied magnetic field, both with and without a control current. In all cases the pattern undergoes an essentially rigid shift. We then evaluate the derivative of critical current with respect to field and the size of the shift from a least squares fit. The current gain is the product of these two. Fig. 10 shows these quantities for the two devices as functions of temperature. Values of up to 1.7 are shown. This is a large improvement on our earlier devices, although still some distance short of the Wisconsin group[18] who have obtained gains of up to 3.

The differential output resistance of the device varies significantly with current, as the IV curve is similar to that for the RSJ model with thermal rounding. The largest values are found at operating currents just above I_c. At say 65K the largest value for the five loop device is 1.3Ω. The transresistance is the product of output resistance and current gain, 1.7Ω in this case. The low output impedance would limit the bandwidth over which the device could be matched to a 50Ω load in high frequency applications. If junctions with rather higher values of r_N can be made this will be much easier.

The high temperature I_c-B pattern is relatively easy to interpret as the β values are low. For the four loop device it shows two minor peaks (corresponding to vortices in individual loops), between the major peaks where the number of vortices in the loops are equal, rather than the expected three. Simulations suggest that this is due to flux focusing into the central loops by the rather wide superconducting leadouts.

6. Two dimensional junction arrays

Low T_c two-dimensional arrays have been studied both as a prototype system showing low dimensional phase transitions and as oscillators. Theoretical[19] and experimental[20,21] studies suggest that synchronisation of the Josephson oscillations in the voltage state is much more robust than for series arrays.

We focus on a pair of arrays, grown on the same substrate as the series array mentioned above. One consists of a 50 by 50 array of 10 μm junctions (the coarse array) on 20 μm centres surrounding 10 μm square holes. The other is a 100 by 100 array of 5 μm junctions

on 10 μm centres with 5 μm square holes (nominal dimensions). The overall array size in both cases is 1mm square.

The bias current to the arrays is supplied via a separate resistor of AgAu alloy to each edge node. The superconductor tracks leading from the resistor to the device are crossed by a bar of the same alloy. This is bought out to a bonding pad and leads to the voltage measuring preamplifier. The voltage readout track may cause significant extra damping on the sideways junctions in the end rows of the array. It is not clear what the effects of heavy shunting would be.

The resistance temperature graphs (fig. 11) for the arrays shows the transition of the electrodes and wiring at 92K. The resistance falls with cooling as the strength of the Josephson couplings in the junctions increases. At lower temperatures the IV curve is remains very soft, with differential resistance rising smoothly with voltage. Critical current is not a very well defined concept in such a case, but if we arbitrarily choose a voltage criterion, we find that I_c increases with further cooling.

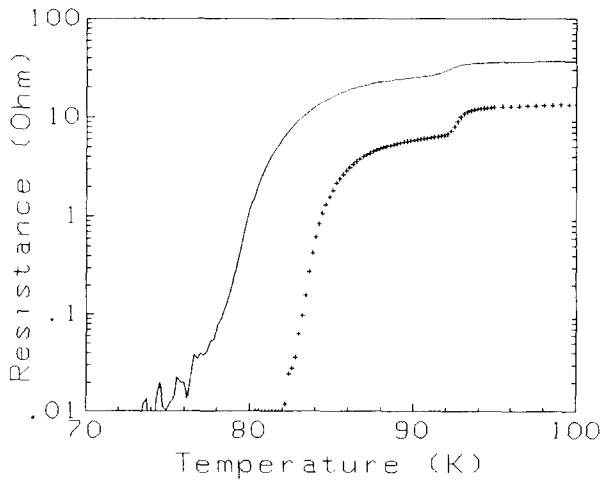

Fig. 11 Resistance of two-dimensional arrays as functions of temperature. Fine array - solid line, coarse array + + +. The measurements were made using a triangular current wave form of about 5μA peak.

At constant temperature the arrays are quite field sensitive. Fig. 12 shows a family of voltage field traces for the fine array at 73K. The main modulation period of 18.5μT is consistent with flux quantisation in an area of 112μm^2, which is in plausible agreement with the array unit cell area of 100μm^2. At low voltages the dips are sharply pointed, evidence for the existence of longer range order than a single loop. The field is frustrating the phase transition. The sign of the modulation reverses at higher voltage. The cause of this is not known, but we have also seen this at least once in a DC-SQUID. Half order dips can also be seen. These could be ascribed to ordered superlattice states, with flux quanta in every other hole. However we should not neglect a more mundane possibility. If a junction is open circuit (or perhaps just very weak), then the loop area is doubled, halving the field period. If a significant minority of such defects exist it may be able to give rise to the half order period. Wider field sweeps show a parabolic background.

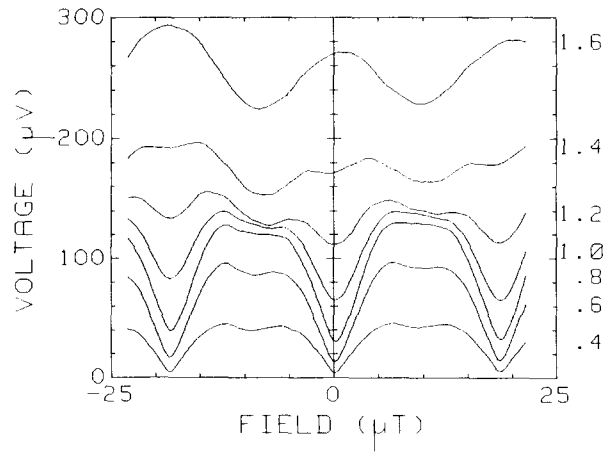

Fig. 12 Voltage vs field for the fine two dimensional array at 73K. For compactness, 0.94 of the zero field voltage has been subtracted from each trace. The bias current in mA is shown to the right of each trace.

The poor matching of critical currents of the series arrays make it quite uncertain whether significant array synchronisation will exist. Most interesting is spontaneous synchronisation, which must be studied in emission. We have not attempted this yet, but we have examined the response to an external microwave field. Giant Shapiro steps at voltages of N2ef/h for an NxN array have been observed in low T_c arrays[21], indicating that all the rows of the junction are synchronised with the external field.

Fig. 13 shows the differential resistance dV/dI as function of voltage for the coarse array. In the absence of microwaves this rises, initially as $|V|$, then curves over towards a constant value. Microwaves tend to suppress the critical current, and lower the differential resistance. In the most favourable case, a broad and rather ill defined minimum in differential resistance occurred at about the right voltage. This was clearest for the coarse array, at a temperature of 82.3K, corresponding to the foot of the resistive transition. At a slightly lower temperature the junction critical currents are somewhat larger, and the single minimum has been replaced by a ripple at the same

voltage and its multiples. We expect that larger microwave powers would show additional structure. Even this, rather weak, evidence for array synchronisation comes as a great surprise, in view of the large spread of critical currents in the junctions. The change in dimensionality has allowed some form of cooperative behaviour, and we suspect that quite modest improvements in junction reproducibility would allow two-dimensional array devices to show much better performance.

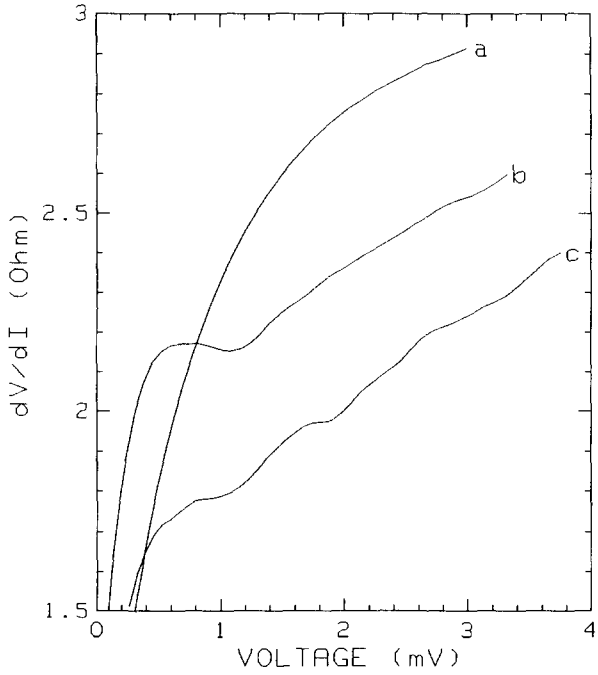

Fig. 13 Differential resistance as a function of voltage for the coarse array. Trace (a) no microwaves 82.2K, (b) 10.12 GHz microwaves, 81.2K, (c) 10.12GHz, 82.3K. The lower temperature unirradiated trace is indistinguishable from (a) in the voltage range shown. $N\Phi_0 f = 1.05$mV is the expected voltage for giant steps.

7. Conclusion

We have described some recent results in the development of high temperature superconductor device technology. The key outstanding problems are insulator leakage and junction reproducibility. Nevertheless, it is now possible to make a range of circuits which show promise, and gain experience of their design and potential.

References

1. S.J.Hedges, N.G.Chew, R.G.Humphreys and S.W.Goodyear. Electronics Lett. 27, 2312 (1991)
2. A.H.Miklich, J.J.Kingston, F.C.Wellstood, J.Clarke, M.S.Colclough, K.Char and G.Zaharchuk. Appl. Phys. Lett. 59, 988 (1991)
3. R.G.Humphreys, N.G.Chew, S.F.Morgan, J.S. Satchell, A.G.Cullis and P.W Smith. Appl. Phys. Lett. 61, 228 (1992)
4. Y.Q.Shen, T.Freltoft and P.Vase. Proc. Int. Conf. Advanced Materials, Strasbourg (1991), France, ed. L.Correra. North Holland. p. 505. We are grateful to Dr. Shen for supplying this sample.
5. R.G.Humphreys, N.G.Chew, J.S.Satchell, S.W. Goodyear, J.A.Edwards and S.E.Blenkinsop. IEEE Trans. Magnetics 27, 1357 (1991)
6. M.N.Keene, S.W.Goodyear, J.S.Satchell, J.A.Edwards, N.G.Chew and R.G.Humphreys. Presented at the Applied Superconductivity Conference, Chicago, 1992
7. H.Obara, S.Kosaka and Y.Kimura. Appl. Pys. Lett. 58, 298 (1991)
8. S.W.Goodyear, J.S.Satchell, R.G.Humphreys, N.G.Chew and J.A.Edwards. Physica C, vol.192, 85 (1992)
9. K.Char, M.S.Colclough, S.M.Garrison, N.Newman, and G. Zaharchuk. Appl. Phys. Lett. 59, 733 (1991)
10. C.L.Jia, B.Kabius, K.Urban, K.Herrman, G.J.Cui, J.Schubert, W.Zander, A.I.Braginski and C.Heiden. Physica C 175, 545 (1991)
11. J.Gao, Y.Boguslavkij, B.B.G.Klopman, D.Terpstra, G.J.Geritsma and H.Rogalla. Appl. Phys. Lett. 59, 2754 (1991)
12. J.A.Edwards, J.S.Satchell, N.G.Chew, R.G. Humphreys, M.N.Keene and O.D.Dosser. Appl. Phys. Lett. 60, 2433 (1992)
13. C.S.Owen and D.J.Scalapino. Phys. Rev. 164, 538 (1967)
14. R.G.Humphreys, J.S.Satchell, J.A.Edwards, N.G.Chew, S.W.Goodyear, M.N.Keene and S.F. Morgan. Presented at the Applied Superconductivity Conference, Chicago 1992.
15. M.N.Keene, S.P.Harrop, T.J.Jackson, C.M.Muirhead and C.E.Gough. Supercond. Sci. Technol. 3, 263 (1990).
16 M.J.Ferrari, J.J.Kingston, F.C.Wellstood and J.Clarke. Appl. Phys. Lett. 58, 1106 (1991)
17. J. S. Satchell, J. A. Edwards, N. G. Chew and R. G. Humphreys. Electronics Lett. 28, 781, (1992).
18. J.S.Martens, D.S.Ginley, J.B.Beyer, J.E.Nordman and G.K.G.Hohenwarter, IEEE Trans. Appl. Superconductivity 1, 95 (1991).
19. M.Octavio, C.B.Whan and C.J.Lobb. Appl. Phys. Lett. 60, 766 (1992).
20. S.P.Benz and C.J.Burroughs. Appl. Phys. Lett. 58, 2162 (1991).
21. S.P.Benz, M.S.Rzchowski, M.Tinkham and C.J. Lobb. Phys. Rev. Lett. 64, 693 (1990).